Achieving the enhanced photocatalytic degradation of ceftriaxone sodium using CdS-g-C3N4 nanocomposite under visible light irradiation: RSM modeling and optimization

Naime AttariKhasraghi
Islamic Azad University

Karim Zare
Islamic Azad University

Ali Mehrizad (✉ ali.mehrizad@yahoo.com)
Islamic Azad University   https://orcid.org/0000-0002-9120-0344

Nasser Modirshahla
Islamic Azad University

Mohammad Ali Behnajady
Islamic Azad University

Research Article

Achieving the enhanced photocatalytic degradation of ceftriaxone sodium using CdS-g-C$_3$N$_4$ nanocomposite under visible light irradiation: RSM modeling and optimization

Abstract

In this research, the cadmium sulfide - graphite carbon nitride (CdS-g-C$_3$N$_4$) nanocomposite was synthesized and characterized by X-ray diffraction (XRD), Field emission scanning electron microscopy (FESEM), energy-dispersive X-ray spectrometer (EDX), and transmission electron microscopy (TEM) techniques. The photocatalytic activity of as-prepared nanocomposite was evaluated in the degradation of ceftriaxone sodium (CTX) antibiotic from aqueous solution under visible light irradiation. The influence of the operational variables such as the amount of photocatalyst (g/L), initial CTX concentration (mg/L), pH, and irradiation time (min) on the photodegradation process was investigated and optimized using response surface methodology (RSM) - central composite design (CCD) model. The maximum degradation percentage (92.55 %) was obtained in the optimal condition, including 0.06 g/L of CdS-g-C$_3$N$_4$ photocatalyst, 15 mg/L of CTX, pH= 10.5, and irradiation time = 81 min. The efficient photocatalytic performance of CdS-g-C$_3$N$_4$ nanocomposite is due to the appropriate alignment of energy levels between the CdS and g-C$_3$N$_4$, which synergistically impact the charge separation and the degradation efficiency of CTX. The kinetics of the photocatalytic degradation process was well described by Langmuir-Hinshelwood's pseudo-first-order model (k_{app} = 0.0336 min^{-1}).

Keywords: Photodegradation, CdS, g-C$_3$N$_4$, Ceftriaxone, RSM, Visible light.

1. Introduction

In recent years, the removal of pharmaceutical compounds from wastewaters has attracted a lot of attention due to their various adverse effects on the environment and human life [1-4]. Medicines, especially antibiotics, accumulate over time due to their high solubility in water and long half-life. Therefore, the mutation of microorganisms will occur, causing the antibiotic-resistant genes, which have dangerous consequences [5-7]. Ceftriaxone (CTX) is a beta-lactam cephalosporin antibiotic having 2-(2-amino-1,3-thiazol-4-yl)-2-(methoxyimino) acetylamino and [(2-methyl-5,6-dioxo-1,2,5,6-tetrahydro-1,2,4-triazin-3-yl)sulfanyl]methyl side-groups that is extensively used to treat various bacterial diseases causes by a wide range of gram-positive and gram-negative bacteria [8, 9]. Ceftriaxone plays an essential role in environmental pollution due to its high use in medicine and veterinary medicine, and may cause bacterial drug resistance, even in low concentrations [10, 11]. Therefore, the purification of the effluents containing ceftriaxone with appropriate, cost-effective, and high-efficiency methods is a challenging issue that researchers have focused on in recent years.

Several procedures can be used to remove antibiotics from water sources [12-15]. Photocatalytic degradation is one of the advanced oxidation processes (AOPs) in which pollutants are destroyed in light radiation and a semiconductor as photocatalyst [16-18]. A suitable photocatalyst should have low band gap energy, high surface area, and good stability [19]. Several inorganic materials (oxides and sulfides) such as TiO_2, ZnO, WO_3, Fe_2O_3, $BiVO_4$, CdS, and ZnS have been developed as semiconductors in photocatalytic removal of antibiotics [20-23]. CdS with a suitable band gap (2.42 eV, visible region), low toxicity, and good thermal and chemical stability is an appropriate candidate for photo-assisted degradation purposes [24-26]. There are a lot of researches about CdS nanostructures used as the photocatalyst in wastewater treatments [27-29]. The application of CdS as a photocatalyst

2

has been limited because of the high recombination of charge carriers (electrons and holes) and low optical stability against light irradiation [30].

Recently, the combination of inorganic metal sulfides with carbon-based materials has been considered a practical approach to overcoming the problem [31]. In this case, the advantages of both organic and inorganic semiconductors improved photocatalytic efficiency due to the fast charge separation and transfer. Among different carbon allotropies, graphitic carbon nitride (g-C$_3$N$_4$) has been attracted lots of attention owing to optoelectrical and chemical properties [32-34]. Chen et al. [35] reported the carboxylic acid - functionalized CdS/g-C$_3$N$_4$ heterojunction as an efficient photocatalyst for sulfamethazine decomposition. The CdS/spherical g-C$_3$N$_4$ photocatalyst was prepared by Wu and Wang et al. [36] using the solvothermal method, which showed 93.2 % tetracycline degradation. Li et al. [37] demonstrated that the Fe$_3$O$_4$/CdS/g-C$_3$N$_4$ photocatalyst had excellent efficiency in the decomposing of the ciprofloxacin under visible light.

Generally, obtaining the optimal conditions for operational parameters in the photocatalytic degradation of pollutants requires several experiments, which are very time consuming and costly. Also in this case, the effect of each variable is discussed independently, while other variables are considered constant and the interaction between the parameters cannot be examined. To overcome the mentioned limitations, the response surface methodology (RSM) method was used for optimizing the photodegradation process. Using RSM as the appropriate mathematical and statistical method, it is possible to provide a model that correlates the various experimental variables (such as the initial concentration of pollutant, pH, irradiation time, the amount of photocatalyst) and the response (photodegradation percentage) obtained by performing fewer tests with greater accuracy. In the RSM category, central composite design (CCD) has been widely used for the optimization of the photocatalytic degradation

process because of the advantage of optimizing multifactor problems with the optimum number of experimental runs [3].

In this project, the CdS-g-C$_3$N$_4$ nanocomposite was synthesized via the chemical precipitation method and applied as an efficient photocatalyst for the decomposition of ceftriaxone (CTX) under visible light irradiation. The degradation process was investigated by the experimental design using RSM based on CCD and the optimal condition obtained considering the interaction and individual effects of input variables (amount of photocatalyst, ceftriaxone concentration, pH, and irradiation time) and their primary influence over time. The process was also examined from a kinetic point of view.

2. Materials and methods

2.1. Synthesis of g-C$_3$N$_4$ powder

The synthesis of g-C$_3$N$_4$ powder was carried out using a calcination process. 5 g melamine (C$_3$H$_6$N$_6$, Merck) was put into a semi-closed crucible and heated in a muffle furnace at 520 ℃ for 4 h. The prepared yellow powder of g-C$_3$N$_4$ was collected and grinned.

2.2. Synthesis of CdS-g-C$_3$N$_4$ nanocomposite

First, 0.0772 gr of as-prepared g-C$_3$N$_4$ powder was dispersed in 50 ml distilled water in the ultrasonic bath for 15 min. Then, 50 ml cadmium chloride monohydrate (CdCl$_2$.H$_2$O, Merck) aqueous solution (0.1 M) and 20 ml methanol (CH$_3$OH, Merck) were added, followed by sonication for 30 min. After that, a 50 ml solution of sodium sulfide (Na$_2$S, Merck) 0.1 M was added gradually into the mixture and stirred for 1h. The obtained precipitate was centrifuged and was washed several times with ethanol and distilled water. Finally, the as-prepared nanocomposite was dried at 80 ℃ in the oven for 2 h and heated in a furnace at 500 ℃ for 1 h.

2.3. Characterization

The crystallographic structures of pure CdS, pure g-C$_3$N$_4$, and as-synthesized CdS-g-C$_3$N$_4$ nanocomposite were evaluated by X-ray diffraction (XRD) analysis using PHILIPS (PW1730, Nederland) with Cu-kα radiation (λ= 1.54 A°, 40 kV, 30 mA). The Field emission scanning electron microscopy (FESEM) (TESCAN, MIRA III) was used for evaluating the morphology of compounds. The elemental composition was determined using an energy dispersive X-ray spectrometer (EDX) (TESCAN, MIRA III equipped with SAMX detector). The transmission electron microscopy (TEM) was done by LEO 906 E (100 kV).

2.4. Investigation of photocatalytic activity

The photocatalytic performance of CdS-g-C$_3$N$_4$ nanocomposite was evaluated by the degradation of ceftriaxone antibiotic under visible light irradiation. All the experiments were performed in a photo reactor equipped with a LED-300 W (OSRAM, Germany) as the light source and a glass optical filter for cut off the components with λ >420 nm.

The CdS-g-C$_3$N$_4$ nanocomposites with different g-C$_3$N$_4$ content (0.00772, 0.0361, 0.0772, 0.1805, and 0.361 gr) were synthesized and their photocatalytic performances in the degradation of CTX were evaluated. The CdS-g-C$_3$N$_4$ nanocomposite containing 0.0772 gr g-C$_3$N$_4$ showed the maximum efficiency for CTX decomposition and selected for the RSM experiment. Before performing each experiment (each run) designed by RSM, the suspensions were magnetically stirred in the dark for 60 min to obtain absorption/desorption equilibrium.

In each test, 100 ml of ceftriaxone solution with appropriate initial concentration and pH along with a certain amount of photocatalyst powder was stirred (250 rpm). The HCl and NaOH solutions (0.1 M) were used for adjusting the pH.

After a specific time, 5 ml of the solution was sampled and centrifuged. The absorbance of ceftriaxone solution was determined by the single-beam UV-Vis spectrophotometer

(Shimadzu UV- Mini-1240) at the $\lambda_{max} = 240$ nm. The percentage of ceftriaxone degradation was calculated by Eq. 1.

Degradation percentage (%) = $(\frac{C_0 - C_t}{C_0}) \times 100$

(1)

where C_0 and C_t are the ceftriaxone concentrations (mg/L) at initial time (t=0) and after a certain irradiation time (t), respectively.

2.5. Experimental design

The photocatalytic analysis was performed according to the experiments designed by Design-Expert®11 software using central composite design (CCD) based on response surface methodology (RSM).

In this regard, four variables (amount of CdS-g-C$_3$N$_4$ photocatalyst (g/L), initial concentration of ceftriaxone (mg/L), pH, and irradiation time (min)) in five levels were chosen according to Table 1.

Table 1. Levels of the operational parameters.

variables	levels				
A: [CdS-g-C$_3$N$_4$] (g/L)	0.01	0.03	0.05	0.07	0.09
B: [CTX] (mg/L)	5	10	15	20	25
C: pH	3	5	7	9	11
D: Time (min)	20	45	70	95	120

The 30 experiments (30 runs) were designed and performed based on operational variables. The designed experiments, along with the actual and predicted results, were presented in Table 2. To evaluate the effect of each variable, a quadratic polynomial model was proposed as a function of independent variables (operational variables) and measured response (degradation percentage) with the general equation as follows (Eq. 2) [38]:

$$y = \beta_0 + \sum_{i=1}^{k} \beta_i X_i + \sum_{i=1}^{k} \beta_{ii} X_i^2 + \sum_{i=1}^{k} \sum_{j=1}^{k} \beta_{ij} X_i X_j + \varepsilon$$

(2)

6

where y is the predicted degradation percentage (%), β_0 is the constant, β_i, β_{ii}, and β_{ij} are the linear, quadratic, and mutual coefficients, respectively. X_i and X_j are the operational variables. X_i^2 and X_iX_j show the quadratic and mutual effects of operational variables, respectively. ε is the residual value related to the experiments [38]. Analysis of Variance (ANOVA), p- value, and F- value were used for statistical analysis of the results.

Table 2. Designed experiments along with the actual and predicted results.

Std.	Run	A: [CdS-g-C₃N₄] (g/L)	B: [CTX] (mg/L)	C: pH	D: Time (min)	R (%) Actual	R (%) predicted
2	1	0.07	10	5	45	69.39	69.22
21	2	0.05	15	3	70	72.89	72.79
1	3	0.03	10	5	45	64.64	65.10
23	4	0.05	15	7	20	61.32	60.92
19	5	0.05	5	7	70	65.81	66.20
16	6	0.07	20	9	95	85.19	85.21
8	7	0.07	20	9	45	66.15	65.52
11	8	0.03	20	5	95	67.29	67.16
26	9	0.05	15	7	70	68.06	67.64
7	10	0.03	20	9	45	54.46	55.21
22	11	0.05	15	11	70	86.46	87.02
18	12	0.09	15	7	70	66.19	65.95
24	13	0.05	15	7	120	79.39	80.25
29	14	0.05	15	7	70	68.25	67.64
4	15	0.07	20	5	45	66.79	67.61
10	16	0.07	10	5	95	63.41	63.15
28	17	0.05	15	7	70	68.33	67.64
3	18	0.03	20	5	45	66.17	65.56
25	19	0.05	15	7	70	65.11	67.64
17	20	0.01	15	7	70	56.53	57.23
9	21	0.03	10	5	95	65.06	64.74
12	22	0.07	20	5	95	63.55	63.50
27	23	0.05	15	7	70	69.95	67.64
15	24	0.03	20	9	95	81.38	80.61
6	25	0.07	10	9	45	69.38	69.70
30	26	0.05	15	7	70	66.11	67.64
5	27	0.03	10	9	45	58.52	57.62
14	28	0.07	10	9	95	88.05	87.72
13	29	0.03	10	9	95	81.38	81.05

| 20 | 30 | 0.05 | 25 | 7 | 70 | 64.07 | 64.14 |

3. Results and discussion

3.1. Characterization

The phase and crystallographic structures of the pure CdS, pristine g-C_3N_4, and CdS-g-C_3N_4 nanocomposite were studied by the XRD analysis (Fig. 1).

<Fig.1>

Fig. 1 (a) illustrates the XRD pattern of the pure CdS. The diffraction peaks at 2θ 24.71, 26.46, 28.16, 36.61, 43.71, 47.86, 51.91, 71.11, and 75.51 are related to (100), (002), (101), (102), (110), (103), (112), (203), and (211) crystal planes of hexagonal wurtzite structure (JCPDS data card No. 41-1049) [39]. Two peaks of g-C_3N_4 were observed at 2θ 13.31° (100) and 27.42° (002), which are assigned to tri-s-triazine units and interlayer stacking of the conjugated double bonds, respectively (Fig.1 (b)) [40, 41]. It can be seen that the XRD patterns of pure CdS and CdS-g-C_3N_4 are similar which is in good agreement with the literatures [42, 43]. It is considered that the intensity of (002) peak in the XRD pattern of the CdS-g-C_3N_4 nanocomposite (Fig. 1 (c)) has increased compared to pure CdS. The relative intensities of diffraction peaks are related to the crystal growth orientation. Therefore, increasing the (002) intensity in the XRD pattern of CdS-g-C_3N_4 nanocomposite is assigned to the growth orientation change of CdS in the presence of g-C_3N_4 due to the formation of the close interface and interactions between the g-C_3N_4 and CdS [43].

The FE-SEM images, together with EDX results of the compounds, were depicted in Fig.2. According to Fig.2 (a_1), the irregular-shaped CdS nanoparticles can be observed with high aggregation due to the high density of particle growth.

From Fig. 2 (b_1), the pristine g-C_3N_4 has irregular wrinkled sheets with a lamellar structure in which layers are stacked together. In the case of CdS-g-C_3N_4 nanocomposite (Fig. 2 (c_1)), the irregular dispersion of high-density CdS nanoparticles in the g-C_3N_4 sheets can be seen,

8

which makes appropriate interfacial connections for efficient charge separation and transfer. The presence of corresponding peaks for each compound in EDX spectra declared the formation of them.

<Fig.2>

The synthesis of CdS-g-C$_3$N$_4$ nanocomposite is also characterized by transmission electron microscopy. TEM image of CdS-g-C$_3$N$_4$ nanocomposite was illustrated in Fig. 3 showing that the CdS nanoparticles distribute irregularly on the g-C$_3$N$_4$ layers.

<Fig.3>

The bang gap energy of synthesized CdS-g-C$_3$N$_4$ nanocomposite was determined using UV-Vis spectroscopy. The UV-Vis absorption spectrum of CdS-g-C$_3$N$_4$ nanocomposite was illustrated in Fig 4.

<Fig.4>

The band gap energy (E$_g$) value are determined from the extrapolating of the linear parts of the $(Ah\nu)^2$ versus $h\nu$ according to $(Ah\nu)^2 = B (h\nu - E_g)$ Tauc-Mott's equation where A is the absorbance (a.u.), $h\nu$ is the photon energy (eV), B is the proportional constant, E$_g$ is the band gap energy (eV) [25]. According to Fig. 4 (b), the Eg of CdS-g-C$_3$N$_4$ nanocomposite was obtained 2.45 eV.

3.2. Photocatalytic degradation: modeling and optimization

The photocatalytic activity of CdS-g-C$_3$N$_4$ was studied in the degradation of CTX under visible light irradiation using the CCD-RSM model. After performing 30 experiments proposed by the software (Table 2), the mathematical model (quadratic polynomial model) was presented as a function of operational parameters and the percentage of ceftriaxone degradation in terms of coded factors as Eq. 3.

Degradation (%) = 67.64 + 2.18 A -0.51 B + 3.56 C + 4.83 D -0.52 AB + 2.07 AC -1.43 AD -

0.72 BC +0.49 BD + 5.95 CD -1.51 A^2 -0.62 B^2 + 3.07 C^2 +0.74 D^2

(3)

To evaluate the accuracy of the proposed model, ANOVA results were used according to

Table 3. The F-value of the model is 102.97 and the p-value of the model is less than 0.0001

indicating the excellent adequacy of the proposed model.

The Predicted R^2 of 0.9720 is in reasonable agreement with the Adjusted R^2 of 0.9801 (i.e.,

the difference is less than 0.2).Therefore, this model can be used to predict the degradation

percentage of ceftriaxone using CdS-g-C$_3$N$_4$ photocatalyst. Considering the ANOVA results

(Table 3) and removing the non-significant terms, Eq. 3 was simplified to Eq. 4.

Degradation (%) = 67.64 + 2.18 A + 3.56 C + 4.83 D + 2.07 AC -1.43 AD -0.72 BC + 5.95

CD   -1.51 A^2 -0.62 B^2 +   3.07 C^2 +0.74 D^2

(4)

The normality of the data is one of the most critical assumptions that must be considered in

any experiment and variance analysis. If the residuals have a typical distribution with zero

mean and constant variance and also the residuals are independent, the analysis is performed

and the adequacy of the proposed model is confirmed.

Table 3. ANOVA results of the designed model.

Source	Sum of squares	Degrees of freedom (Df)	Mean square	F-value	p-value Prob > F
Model	2062.11	14	147.29	102.97	< 0.0001, significant
A- [CdS- g-C$_3$N$_4$]	114.10	1	114.10	79.77	< 0.0001
B- [CTX]	6.33	1	6.33	4.43	0.0526
C-pH	303.53	1	303.53	212.20	< 0.0001
D-Time	560.18	1	560.18	391.63	< 0.0001
AB	4.25	1	4.25	2.97	0.1052
AC	68.27	1	68.27	47.73	< 0.0001
AD	32.58	1	32.58	22.77	0.0002
BC	8.19	1	8.19	5.73	0.0302
BD	3.87	1	3.87	2.71	0.1207

CD	566.08	1	566.08	395.75	< 0.0001
A^2	62.67	1	62.67	43.81	< 0.0001
B^2	10.43	1	10.43	7.29	0.0165
C^2	258.04	1	258.04	180.40	< 0.0001
D^2	14.91	1	14.91	10.42	0.0056
Residual	21.46	15	1.43		
Lack of Fit	6.35	10	0.64	0.21	0.9825 not significant
Pure Error	15.10	5	3.02		
Cor Total	2083.57	29			
Predicted R^2 = 0.9720			Adjusted R^2 = 0.9801		

The normal plot of residuals vs. internally residuals was illustrated in Fig. 5.

<Fig.5>

As can be seen, the points are on a straight line and the distribution of the residuals has a slight deviation. Therefore, the error variance is homogeneous and there is no obvious scatter. Examining data independence is another factor that should be considered regarding the adequacy of the model. In this regard, the plot of residuals versus run was shown in Fig. 6.

<Fig.6>

According to Fig. 6, this plot does not show a specific trend. The selected model is valid for examining the relationship between the obtained response and the selected independent variables.

Considering Eq. 4, the three-dimensional (3D) response surfaces diagrams (response levels) related to the effects of variables (amount of photocatalyst, pH and irradiation time) on the response (percentage of degradation) are shown in Fig. 7.

<Fig.7>

The response surface diagram in Fig. 7 (a) shows the effect of the concentration of CdS-g-C_3N_4 nanocomposite (A) and the irradiation time (D) on the CTX degradation percentage. The two parameters of initial antibiotic concentration and pH are 10 mg/L and 9,

respectively. It is observed that with increasing the concentration of photocatalyst and the irradiation time, the percentage of degradation also increases.

As the irradiation time and the amount of photocatalyst increases, the amount of produced electrons and holes increases, resulting in more active species (OH$^.$, O$_2^{.-}$) being formed and the degradation efficiency increases.

pH is one of the effective parameters in the photocatalytic degradation of CTX. As shown in Fig. 7 (b) and 7 (c), the degradation efficiency increases as the pH becomes alkaline. According to the literatures [8, 44], high degradation efficiency of CTX in alkaline condition can be influenced by two factors. With increasing pH, the amount of OH$^-$ ions increased which eventually led to an increase in OH$^.$ [8, 44]. Also, in alkaline pH, hydrolysis of CTX is intensified due to the instability of the beta-lactam ring [45].

After investigating the role of operational variables, an optimization process was performed. The results proposed that 92.55 % of CTX antibiotic degrades at the initial CTX concentration of 15 mg/L, 0.06 g/L of CdS-g-C$_3$N$_4$ photocatalyst, pH = 10.5, and 81 min visible light irradiation. The experimental analysis was carried out under the proposed optimal condition and 91.97% was obtained for photodegradation of CTX antibiotic. It is considered that the observed photodegradation percentage is in good agreement with the predicted theoretical value, which confirmed the validity of the model.

3.3. Photodegradation mechanism

The photodegradation mechanism for CTX decomposition using CdS-g-C$_3$N$_4$ photocatalyst under visible light was schematically shown in Fig. 8. The electrons of CdS and g-C$_3$N$_4$ were excited simultaneously during visible light. The relevant energy correspondence between CdS and the g-C$_3$N$_4$ caused the transmission of the electrons from the conduction band (CB) of g-C$_3$N$_4$ (-1.11 eV vs. NHE) to the CB of CdS (-0.26 eV vs. NHE) and the holes from the valence band (VB) of CdS (1. 98 eV vs. NHE) to the VB of g-C$_3$N$_4$ (1.54 eV vs. NHE).

Therefore, the CdS and g-C$_3$N$_4$ formed the type -II heterojunction photocatalyst system, which accelerated the separation of charge carriers. The rapid transfer of charge carriers and their effective separation from each other, which ultimately leads to an increase in the degradation efficiency of CTX.

The CB of CdS and g-C$_3$N$_4$ is agreeable with the redox potential of O$_2$/O$_2^-$(-0.046 eV vs. NHE). So, the electrons of CB in the CdS and g-C$_3$N$_4$ produce superoxide anions (O$_2^-$). The electrons in the CB of CdS and g-C$_3$N$_4$ reacted with the O$_2$ molecules and H$^+$, producing hydrogen peroxide (H$_2$O$_2$). The H$_2$O$_2$ produced OH$^.$, which reacted with CTX molecules and produced CO$_2$, H$_2$O. On the other hand, produced holes will be directly reacted with CTX molecules [27].

<Fig.8>

According to the proposed mechanism, superoxide radicals (O$_2^-$), hydroxide radicals (OH$^.$), and produced holes (h$^+$) are the main species in the photocatalytic degradation of the antibiotic ceftriaxone. Based on the literatures, OH$^.$ and h$^+$ were more active than O$_2^-$ for decomposition of CTX in the presence of g-C$_3$N$_4$ nanocomposites [46].

3.4. Kinetic studies

To evaluate the kinetics of the photocatalytic removal of ceftriaxone in the presence of CdS-g-C$_3$N$_4$ nanocomposite, the experiments were performed under the optimal conditions proposed by the software for 80 min. The Langmuir-Hinshelwood (L-H) model [47] (Eq. 5), one of the most common kinetic models for the study of heterogeneous photocatalytic systems, was used to investigate the process kinetics.

$$R = -\frac{dC}{dt} = \frac{kKC}{1+KC_0}$$

(5)

Where R is reaction rate, k is the reaction rate constant (min^{-1}mgL^{-1}), K is the adsorption equilibrium constant (Lmg^{-1}), t is the irradiation time (min), C$_0$ and C$_t$ are the pollutant

13

concentrations (mgL^{-1}) at the beginning and time t, respectively. By integrating Eq. 6 and defining the apparent rate constant (k$_{app}$), the equation becomes quasi-first-order kinetics (Eq.7) [48].

$$Ln \frac{C_0}{C_t} = -k_{app} \, t \tag{6}$$

The $Ln \frac{C_0}{C_t}$ vs. irradiation time (t) diagram was illustrated in Fig. 9. Using the slope of Fig. 9, k$_{app}$ was obtained for the photocatalytic degradation of CTX under optimal conditions equal to 0.0336 min^{-1}.

<Fig.9>

4. Conclusion

In this study, the efficiency of the as-synthesized CdS-g-C$_3$N$_4$ nanocomposite for photocatalytic removal of the ceftriaxone antibiotic under visible light was modeled and optimized using the response surface methodology-central composite design (RSM-CCD) model. The results showed that the amount of photocatalyst [CdS-g-C$_3$N$_4$], pH and irradiation time are the most influential the degradation efficiency factors. The higher the amount of these factors, the higher the decomposition efficiency. The highest percentage of degradation (92.55%) was obtained in the initial concentration of ceftriaxone 15 mg/L, in the presence of 0.06 g/L of photocatalyst, pH = 10.5, and irradiation time of 81 min as optimal conditions. Process kinetics evaluation also showed that the photocatalytic removal of ceftriaxone in the optimal conditions proposed by the software follows the quasi-first-order model with an apparent rate constant of 0.0336 min^{-1}. The straightforward synthesis of CdS-g-C$_3$N$_4$ nanocomposite (chemical precipitation) and its high performance in the photocatalytic degradation of ceftriaxone under visible light make it recommended for treating effluents containing this drug.

14

Declaration of interests

The authors declare that they have no known competing financial interests or personal relationships that could have appeared to influence the work reported in this paper.

References

1.   S. Majumder, S. Chatterjee, P. Basnet and J. Mukherjee, Environ. Nanotechno. Monit. Manag. **14**, 100386 (2020).

2.   N. Ahmadpour, M. H. Sayadi, S. Sobhani and M. Hajiani, J. Environ. Manage. **271**, 110964 (2020).

3.   X. Shi, A. Karachi, M. Hosseini, M. S. Yazd, H. Kamyab, M. Ebrahimi and Z. Parsaee, Ultrason. Sonochem. **68**, 104460 (2020).

4.   X. He, V. Nguyen, Z. Jiang, D. Wang, Z. Zhu and W.-N. Wang, Catal. Sci. Technol. **8**, 2117 (2018).

5.   J. Hong, D. K. Hwang, R. Selvaraj and Y. Kim, J. Ind. Eng. Chem. **79**, 473 (2019).

6.   M. J. F. Calvete, G. Piccirillo, C. S. Vinagreiro and M. M. Pereira, Coord. Chem. Rev. **395**, 63 (2019).

7.   G. Lofrano, G. Libralato, S. K. Sharma and M. Carotenuto, in Nanotechnologies for Environmental Remediation: Applications and Implications, eds. by G. Lofrano, G. Libralato and J. Brown, (Springer, Cham, 2017), p. 221.

8.   M. Shokri, G. Isapour, S. Shamsvand and B. Kavousi, J. Mater. Environ. Sci. **7**, (2016) 2843.

9.   S. Y. Hashemi, M. Yegane Badi, H. Pasalari, A. Azari, H. Arfaeinia and A. Kiani, Int. J. Environ. Anal. Chem. (2020) http:// doi.org/ 10.1080/03067319.2020.1817909.

10.   Y. Zhao, X. Liang, Y. Wang, H. Shi, E. Liu, J. Fan and X. Hu, J. Colloid Interface Sci. **523**, 7 (2018).

11.	Y. Zhao, Y. Wang, E. Liu, J. Fan and X. Hu, Appl. Surf. Sci. **436**, 854 (2018).

12.	F. Yu, Y. Sun, M. Yang and J. Ma, J. Hazard. Mater. **374**, 195 (2019).

13.	Y. Gao, Y. Li, L. Zhang, H. Huang, J. Hu, S. M. Shah and X. Su, J. Colloid Interface Sci. **368**, 540 (2012).

14.	E. M. Cuerda-Correa, M. F. Alexandre-Franco and C. Fernández-González, Water, 12 (2020).

15.	Z.-Y. Lu, Y.-L. Ma, J.-T. Zhang, N.-S. Fan, B.-C. Huang and R.-C. Jin, J.Water Process. Eng. **38**, 101681 (2020).

16.	H. Zhao, G. Li, F. Tian, Q. Jia, Y. Liu and R. Chen, Chem. Eng. J. **366**, 468 (2019).

17.	S. Dong, L. Cui, W. Zhang, L. Xia, S. Zhou, C. K. Russell, M. Fan, J. Feng and J. Sun, Chem. Eng. J. **384**, 123279 (2020).

18.	P. Gholami, A. Khataee, R. D. C. Soltani, L. Dinpazhoh and A. Bhatnagar, J. Hazard. Mater. **382**, 121070 (2020).

19.	R. Tangsiri and A. Nezamzadeh-Ejhieh, Chem. Phys. Lett. **758**, 137919 (2020).

20.	O. Sacco, V. Vaiano, L. Rizzo and D. Sannino, Chem.Eng. Process. **137**, 12 (2019).

21.	V. T. Quyen, J. Kim, P.-M. Park, P. T. Huong, N. M. Viet and P. Q. Thang, J. Environ. Chem. Eng. (2020) https://doi.org/10.1016/j.jece.2020.104737.

22.	S. Zhang, J. Yi, J. Chen, Z. Yin, T. Tang, W. Wei, S. Cao and H. Xu, Chem. Eng. J. **380**, 122583 (2020).

23.	K. Zhang, W. Meng, S. Wang, H. Mi, L. Sun and K. Tao, New J. Chem. **44**, 472 (2020).

24.	M. Nagamine, M. Osial, K. Jackowska, P. Krysinski and J. Widera-Kalinowska, J. Mar. Sci. Eng, 8 (2020).

25.	A. G. Khosroshahi and A. Mehrizad, J. Mol. Liq. **275**, 629 (2019).

26.	A. İ. Vaizoğullar, J. Inorg. Organomet. Polym. Mater. **30**, 4129 (2020).

27. B. Shao, X. Liu, Z. Liu, G. Zeng, W. Zhang, Q. Liang, Y. Liu, Q. He, X. Yuan, D. Wang, S. Luo and S. Gong, Chem. Eng. J. **374**, 479 (2019).

28. G. Afreen, M. Shoeb and S. Upadhyayula, Mater. Sci. Eng. C. **108**, 110372 (2020).

29. M. Kaur, S. K. Mehta and S. K. Kansal, J. Environ. Chem. Eng. **6**, 3631 (2018).

30. P. Huo, Y. Tang, M. Zhou, J. Li, Z. Ye, C. Ma, L. Yu and Y. Yan, J. Ind. Eng. Chem. **37**, 340 (2016).

31. M.-f. Li, Y.-g. Liu, G.-m. Zeng, N. Liu and S.-b. Liu, Chemosphere **226**, 360 (2019).

32. L. Wang, K. Wang, T. He, Y. Zhao, H. Song and H. Wang, ACS Sustain. Chem. Eng. **8**, 16048 (2020).

33. T. O. Ajiboye, O. A. Oyewo and D. C. Onwudiwe, J. Inorg. Organomet. Polym. Mater. (2020) http://doi.org/10.1007/s10904-020-01803-3.

34. S. Moorthy, G. Moorthy and K. Swaminathan, J. Inorg. Organomet. Polym. Mater. **30**, 4664 (2020).

35. S. Cao, Z. Jiao, H. Chen, F. Jiang and X. Wang, J. Photochem. Photobiol. A. **364**, 22 (2018).

36. J. Su, X. Wu, C. Zhang, H. Wang, M. Zhang, J. Zhang, Y. Jia, Y. Cui, X. Tong, J. Shang and C. Zhang, J. Wuhan Univ.Technol.Mater. Sci. Ed. **35**, 99 (2020).

37. N. Zhang, X. Li, Y. Wang, B. Zhu and J. Yang, Ceram. Int. **46**, 20974 (2020).

38. E. B. Yazdani and A. Mehrizad, J. Mol. Liq. **255**, 102 (2018).

39. S. Bhalerao, S. Arbuj, S. Rane, J. Ambekar and U. Mulik, Nanosci. Nanotechnol. Lett. **6**, 204 (2014).

40. M. B. Shekardasht, M. H. Givianrad, P. Gharbani, Z. Mirjafary and A. Mehrizad, Diam. Relat. Mater. **109**, 108008 (2020).

41. B. Tahir, M. Tahir, N. Aishah and N. A. Saidina Amin, Chem. Eng. Trans., 56 (2017).

42. Ch. Zhang, Y. Lu, Q. Jiang, J. Hu, Nanotechnology. **27**, 355402 (2016).

43.   X. Liu, Y. Liu, W. Zhang, Q. Zhong, X. Ma, Mate. Sci. Semicond. Process. **105**, 104734 (2020).

44.   C.H. Chiou, C.Y. Wu, R.S. Juang, Chem. Eng. J. **139**, 322 (2008).

45.   M. R. Usman, A. Prasasti, S. Islamiah, A. N. Firdaus, A. W. Marita, S. Fajriyah and E. F. Yanti. J. Kimia Valensi. (2020) http:// doi.org/10.15408/jkv.v6i1.12475.

46.   Y. Zhao, Y. Wang, H. Shi, E. Liu, J. Fan, X. Hu, Mater. Lett. **231**, 150 (2018).

47.   X. Zheng, D. Zhang, Y. Gao, Y. Wu, Q. Liu and X. Zhu, Inorg. Chem. Commun. **110**, 107589 (2019).

48.   H. Kais, N. Y. Mezenner, M. Trari and F. Madjene, Russ. J. Phys. Chem. A. **93**, 2834 (2019).

Figures Caption:

Fig.1. XRD patterns of (a) pure CdS (b) pristine g-C_3N_4 (c) CdS-g-C_3N_4 nanocomposite.

Fig.2. FE-SEM images and EDX results of (a) pure CdS (b) pristine g-C_3N_4 (c) CdS-g-C_3N_4 nanocomposite.

Fig. 3. TEM image of CdS-g-C_3N_4 nanocomposite.

Fig. 4. (a) UV-Vis absorbance spectrum (b) $(Ahv)^2$ vs. hv of CdS-g-C_3N_4 nanocomposite.

Fig. 5. The normal plot of probability vs. internally residuals.

Fig. 6. The plot of residuals versus run numbers.

Fig. 7. Response surface plots of the CTX photodegradation percentage as a function of (a) concentration of CdS-g-C_3N_4 nanocomposite and time (b) concentration of CdS-g-C_3N_4 nanocomposite and pH (c) time and pH.

Fig.8.The schematic illustration of photodegradation mechanism for CTX decomposition using CdS-g-C_3N_4 photocatalyst under visible light.

Fig.9. Ln $\frac{C_0}{C_t}$ vs. time diagram for the photocatalytic degradation of CTX under optimal conditions ([CdS-g-C_3N_4] = 0.06 g/L, [CTX]$_0$= 15 mg/L, pH=10.5).
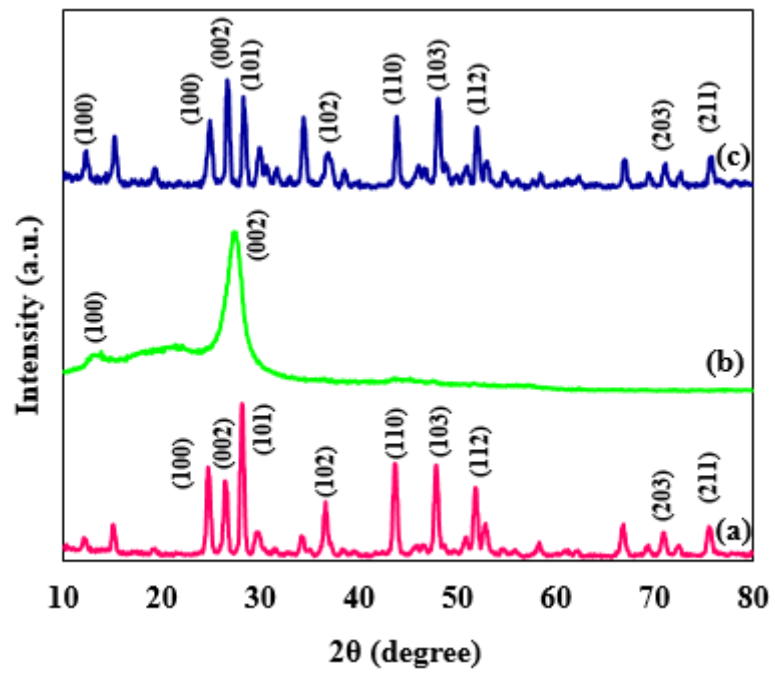
Fig.1.
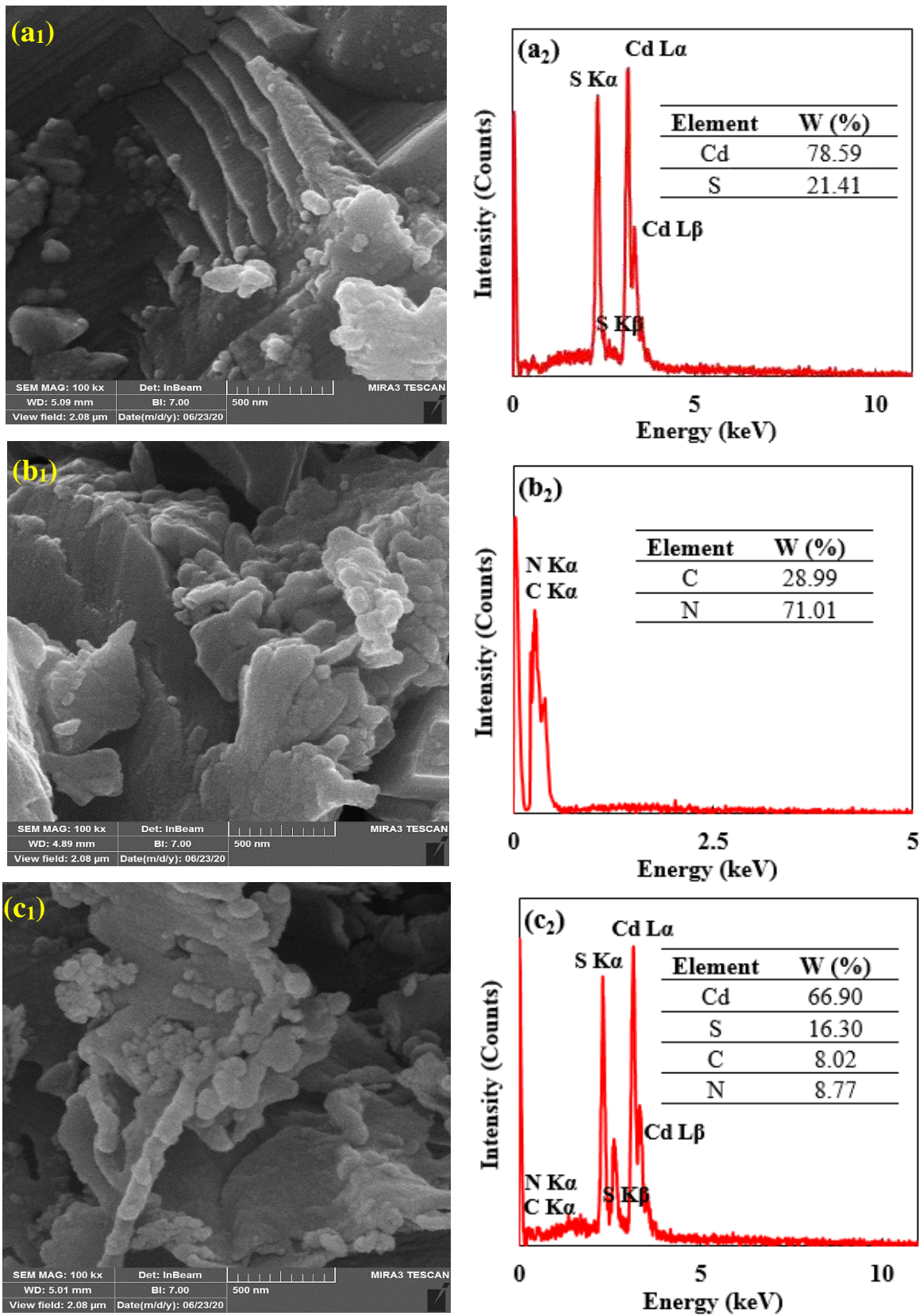
Fig.2.
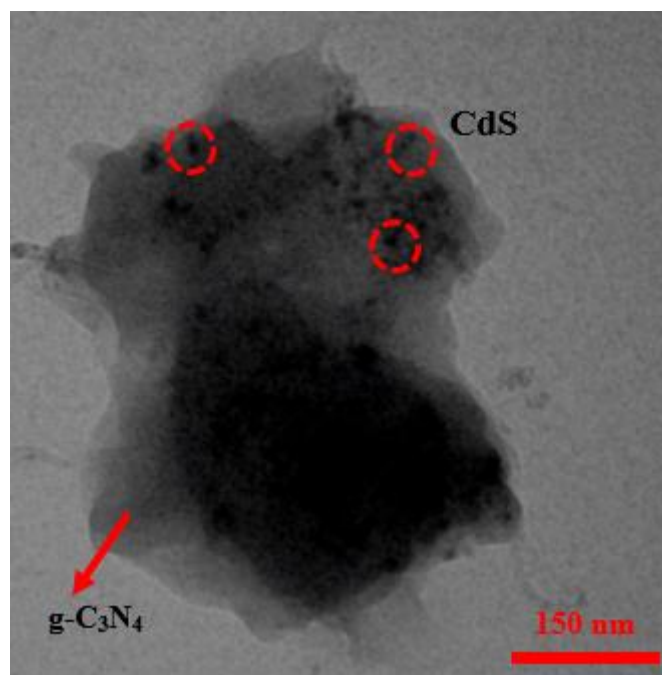
Fig.3.
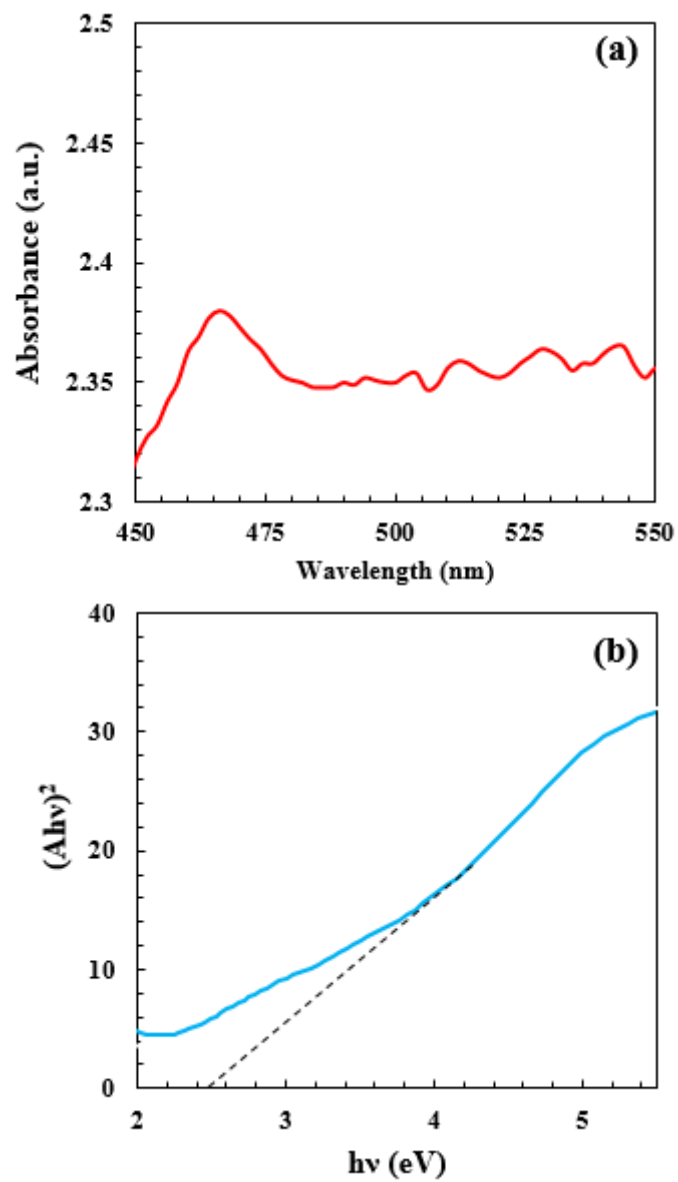
Fig.4.
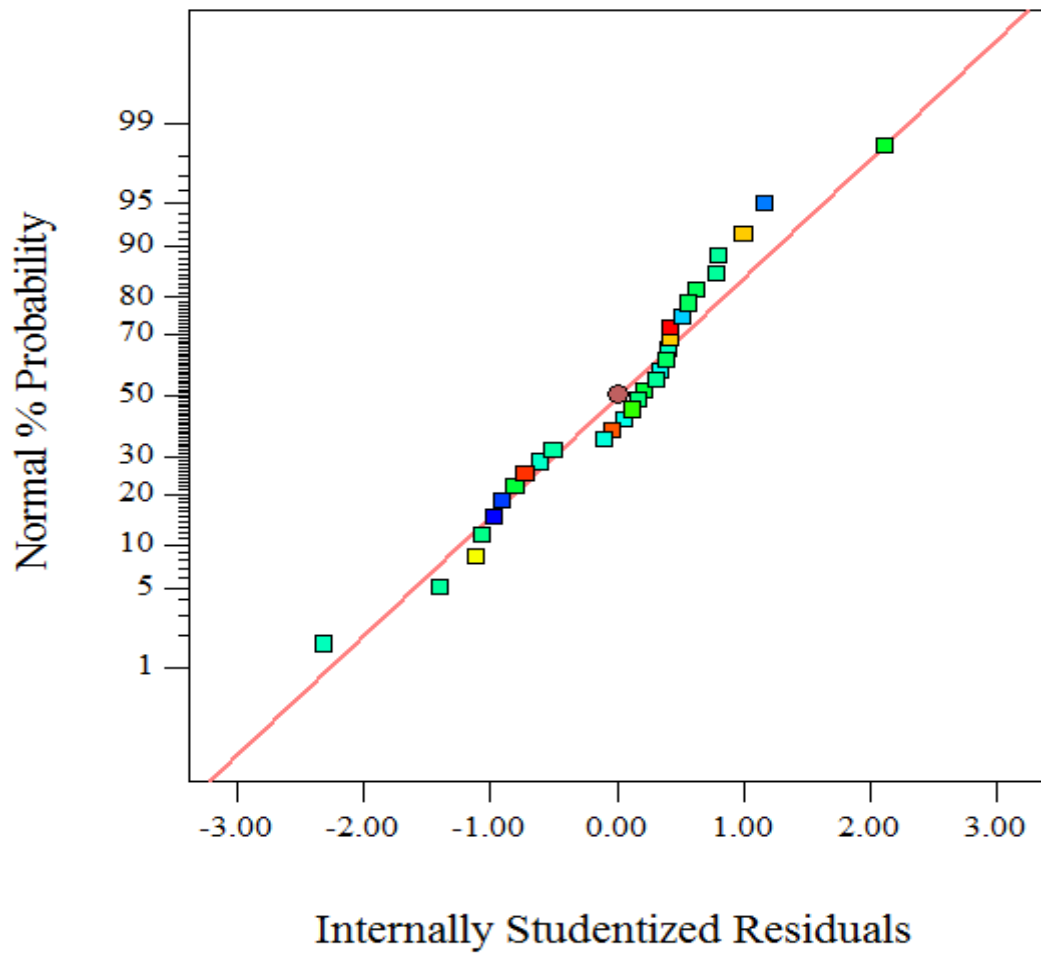
Fig. 5.
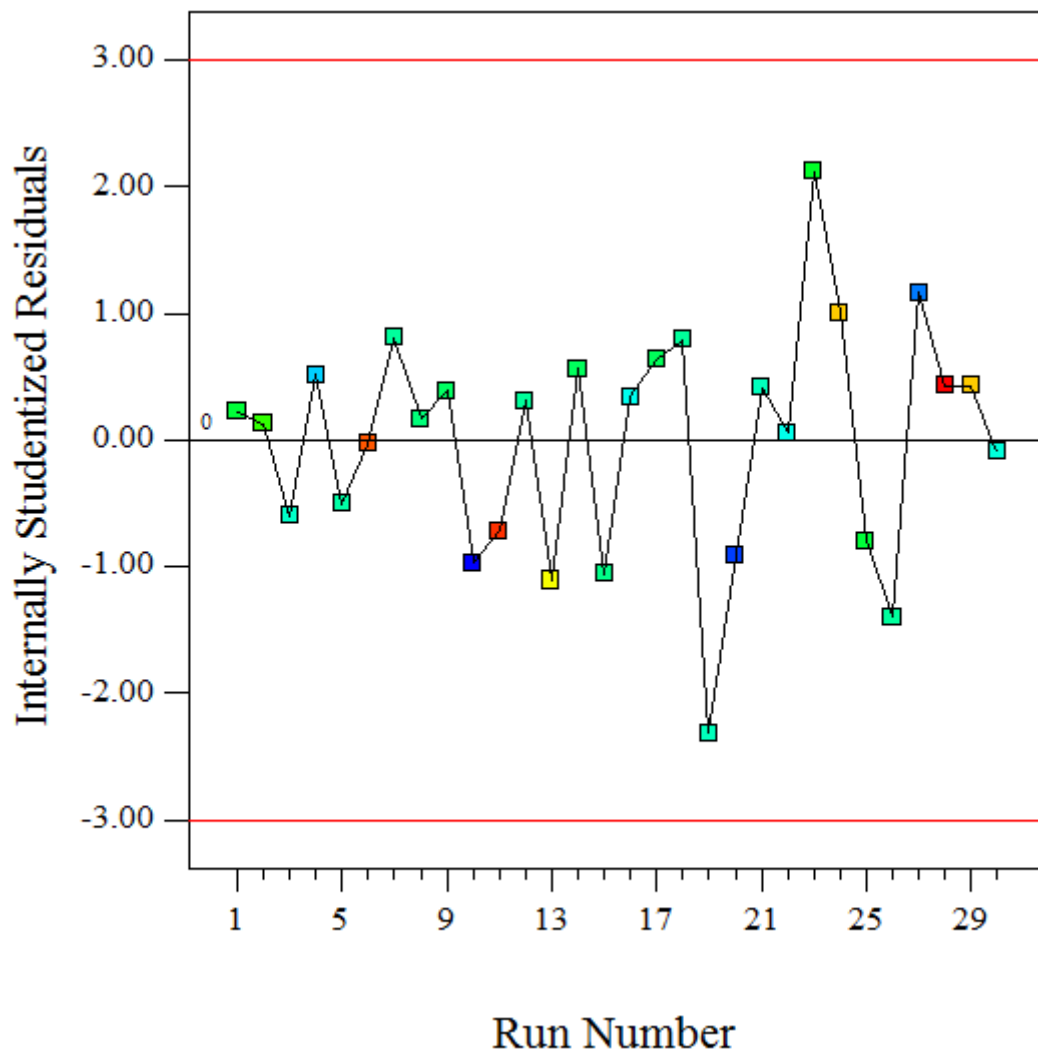
Fig. 6.
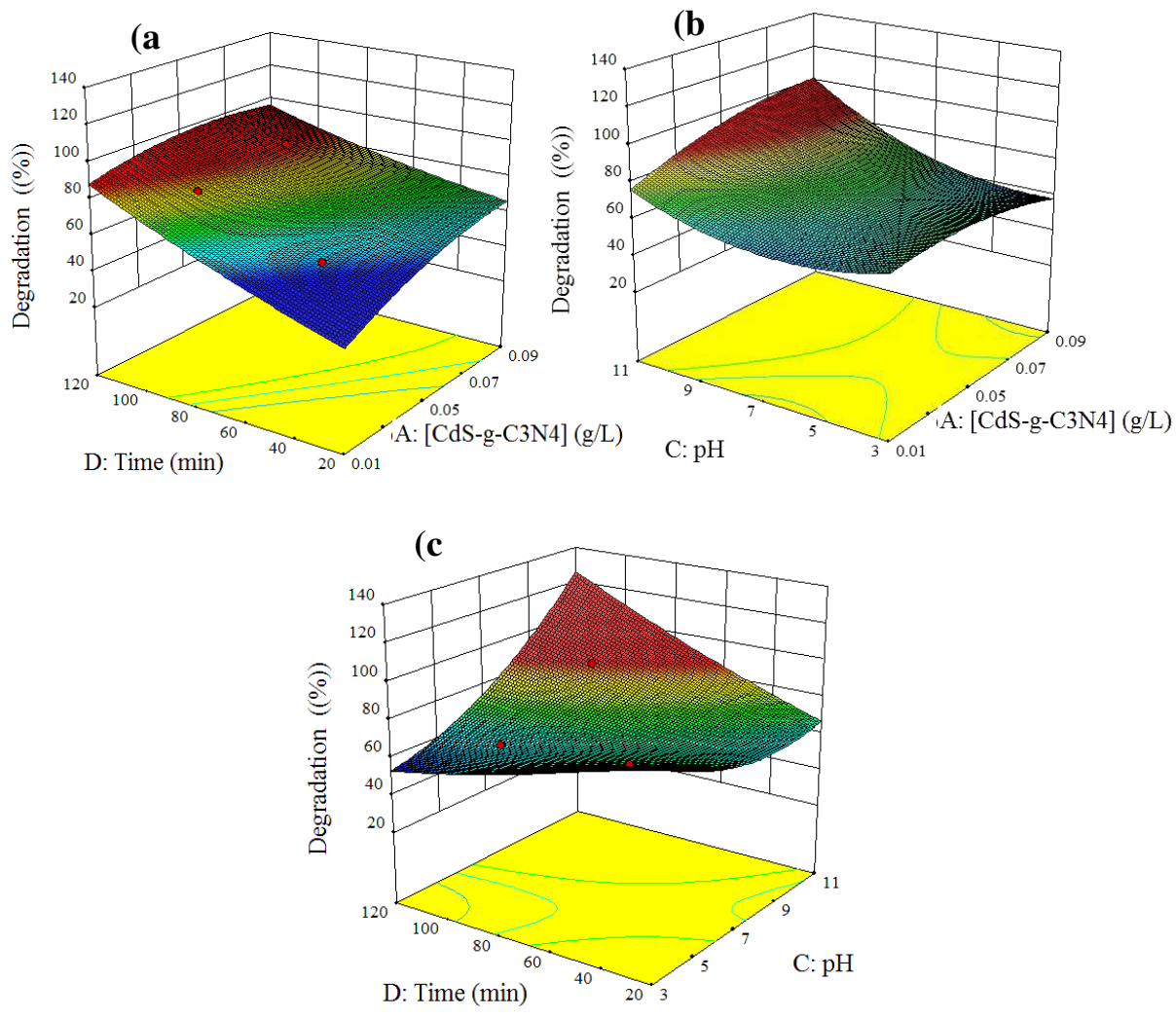
Fig.7.
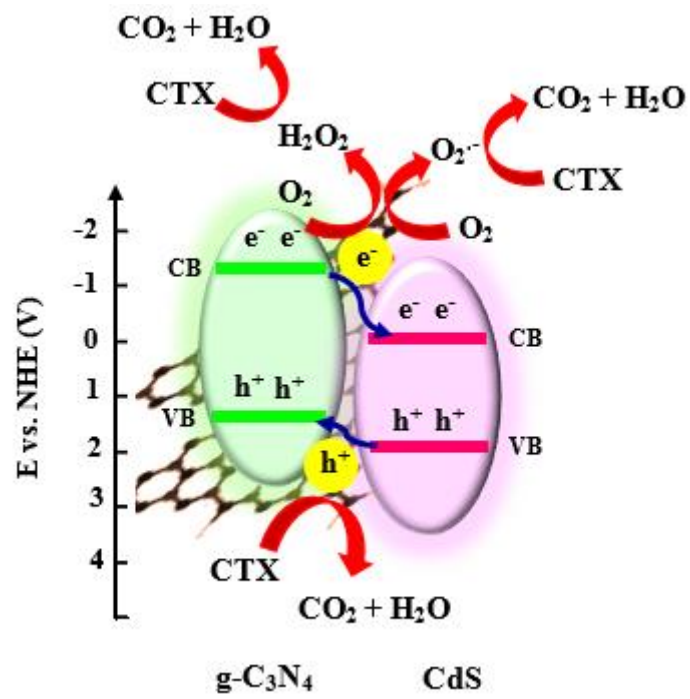
Fig.8.
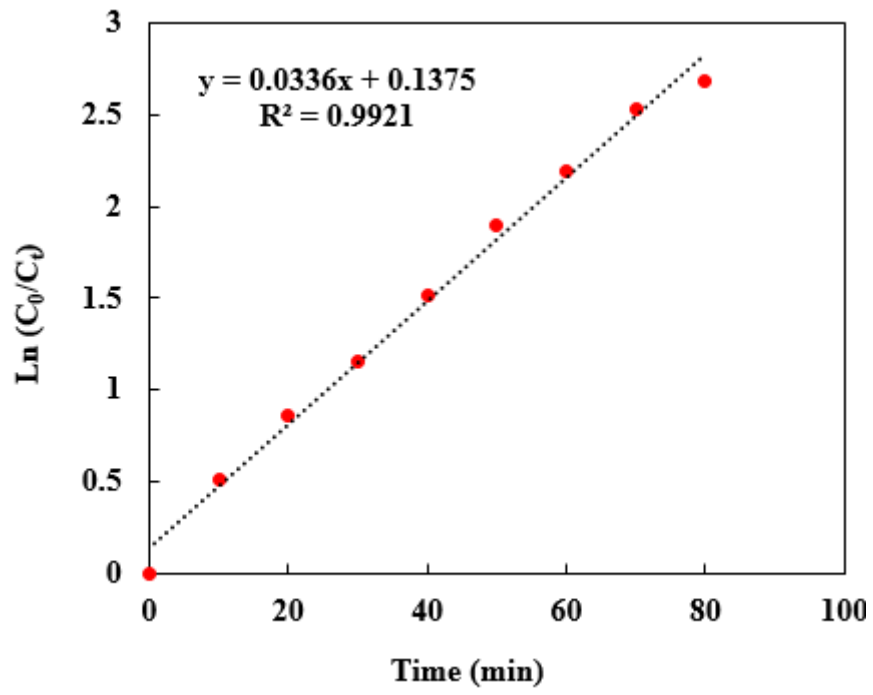
Fig.9.

Figures
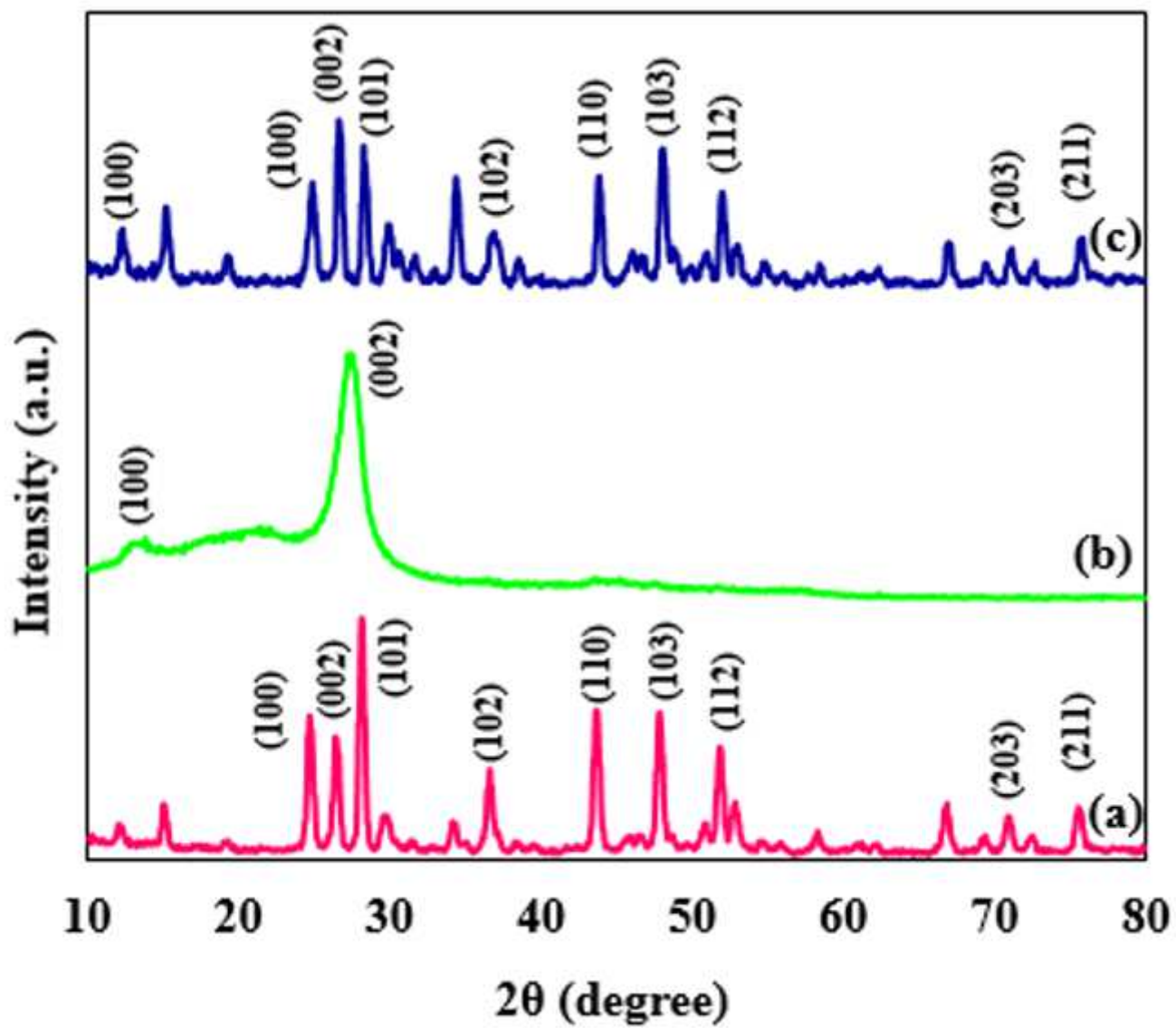
Figure 1

XRD patterns of (a) pure CdS (b) pristine g-C3N4 (c) CdS-g-C3N4 nanocomposite.
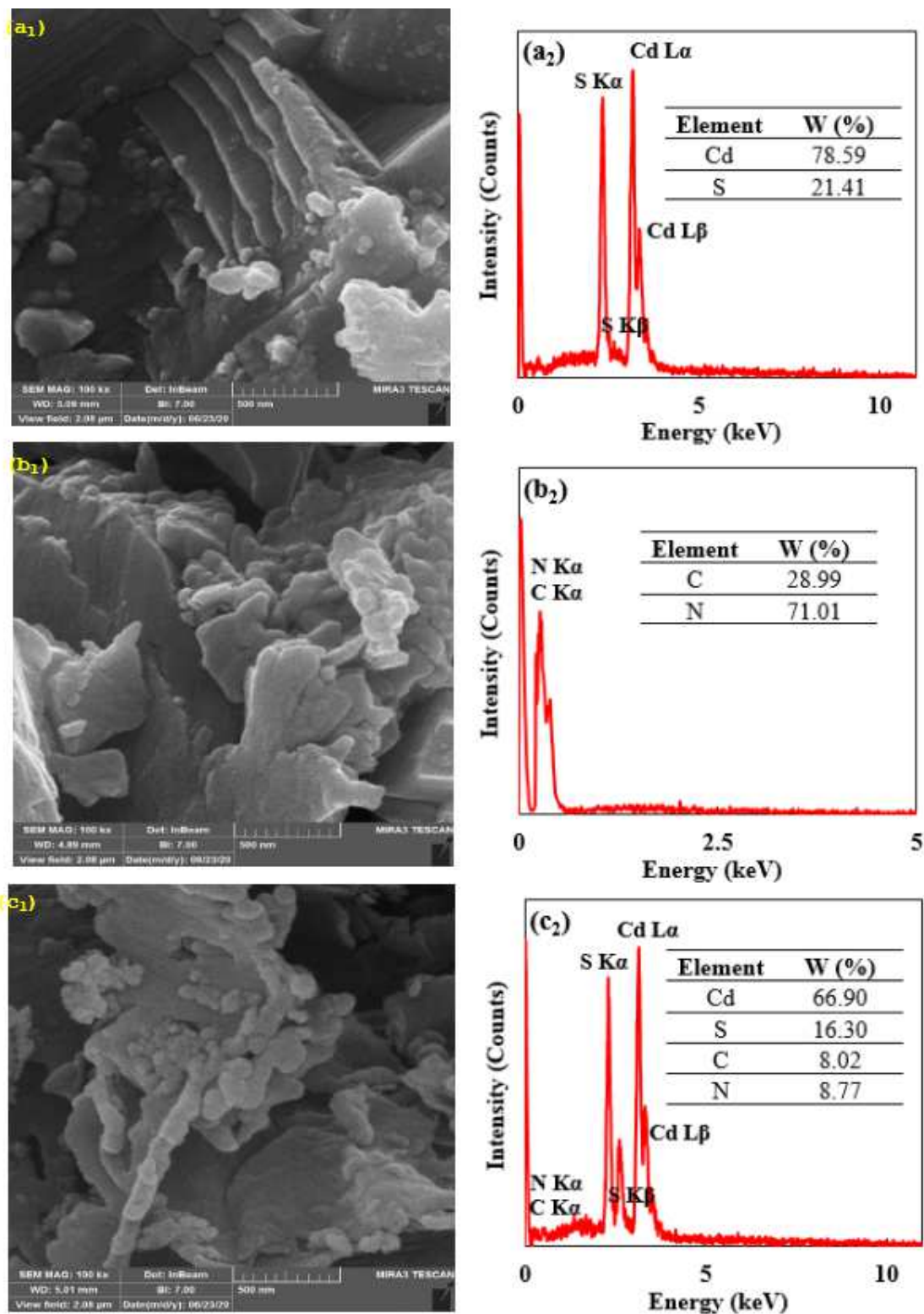
Figure 2

FE-SEM images and EDX results of (a) pure CdS (b) pristine g-C3N4 (c) CdS-g-C3N4 nanocomposite.
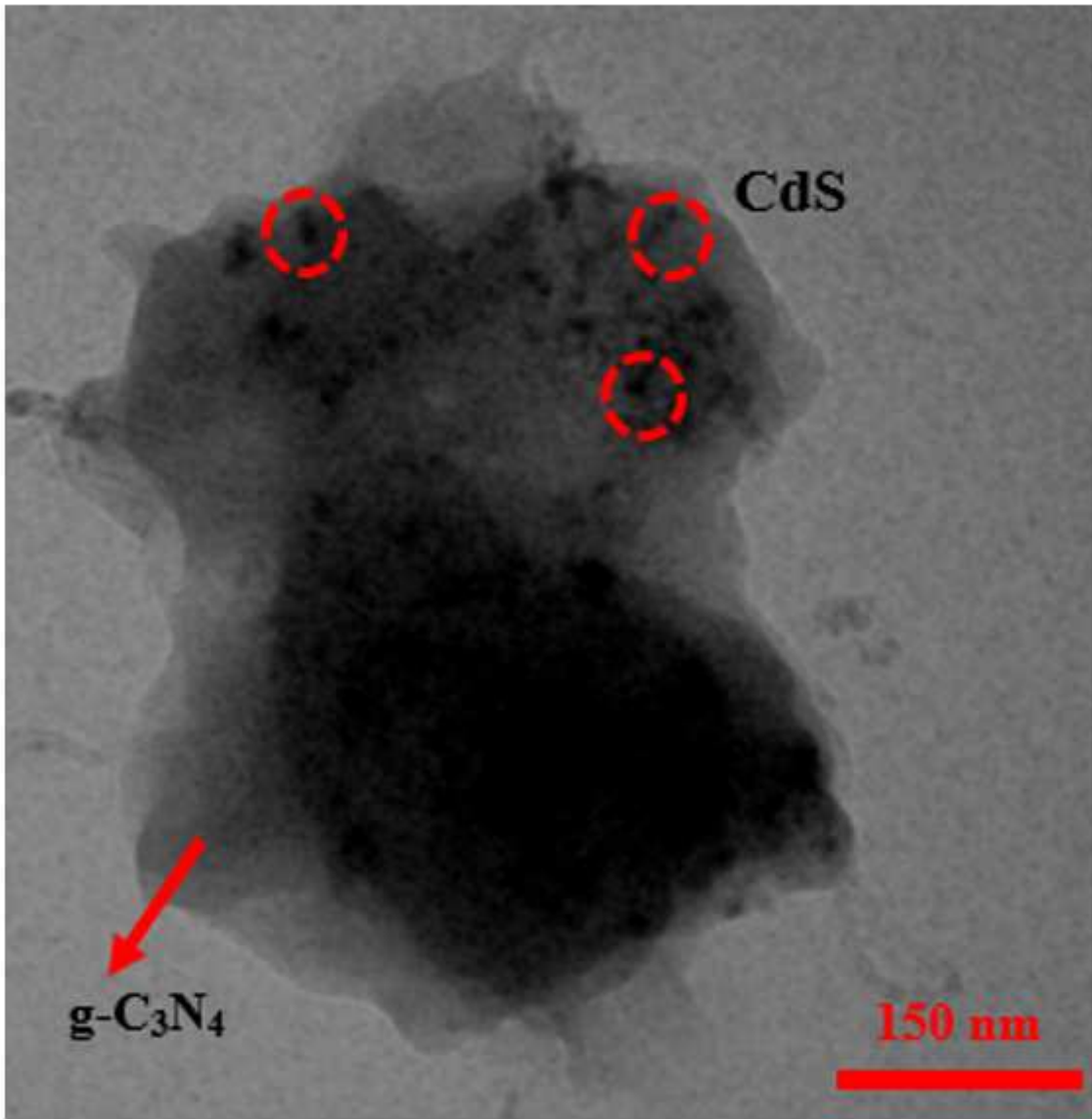
Figure 3

TEM image of CdS-g-C3N4 nanocomposite.
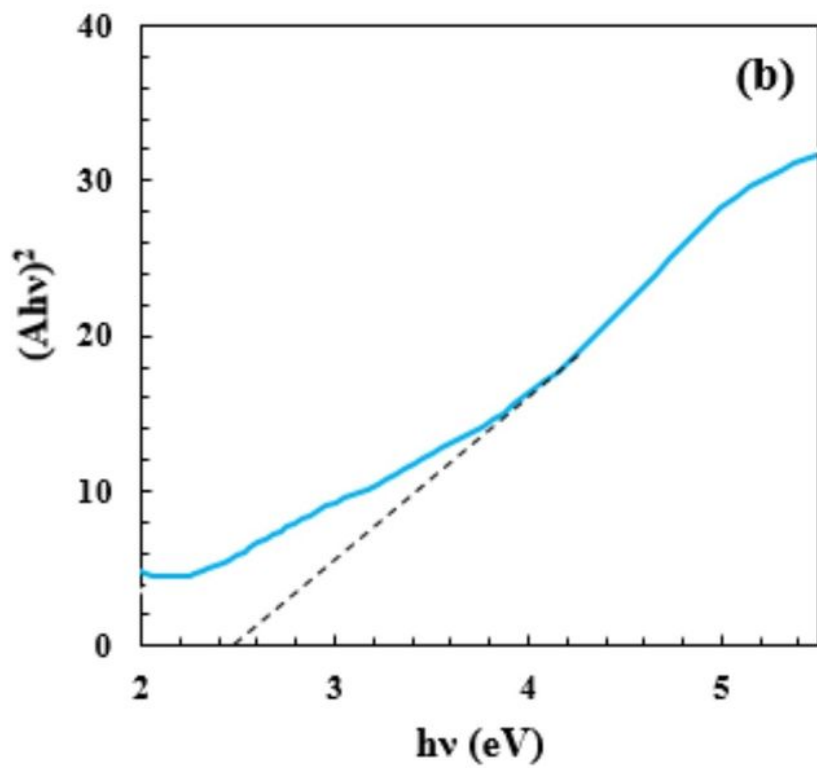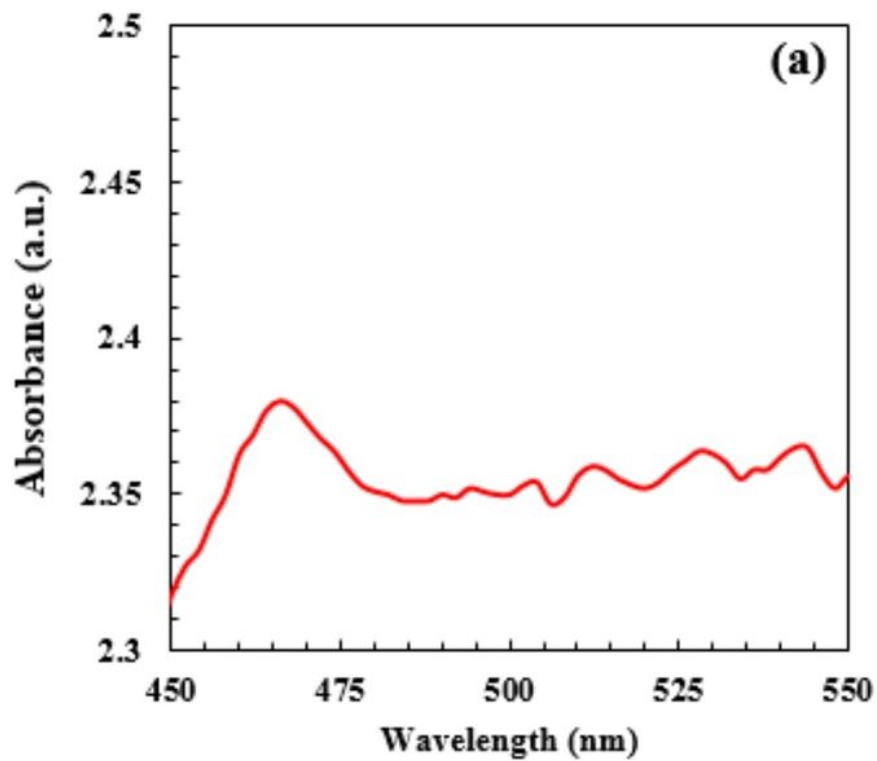
Figure 4

(a) UV-Vis absorbance spectrum (b) (Ahv)2 vs. hv of CdS-g-C3N4 nanocomposite.
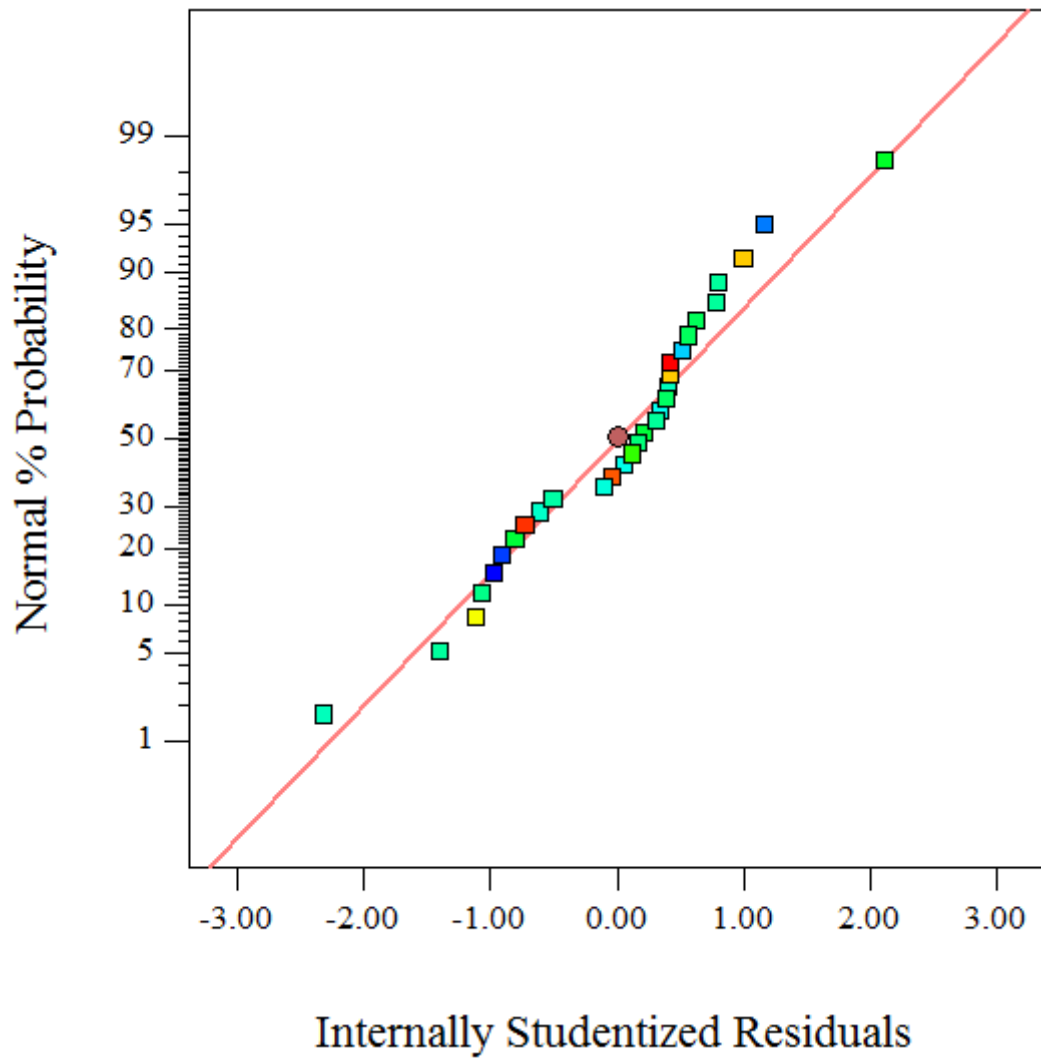
Figure 5

The normal plot of probability vs. internally residuals.
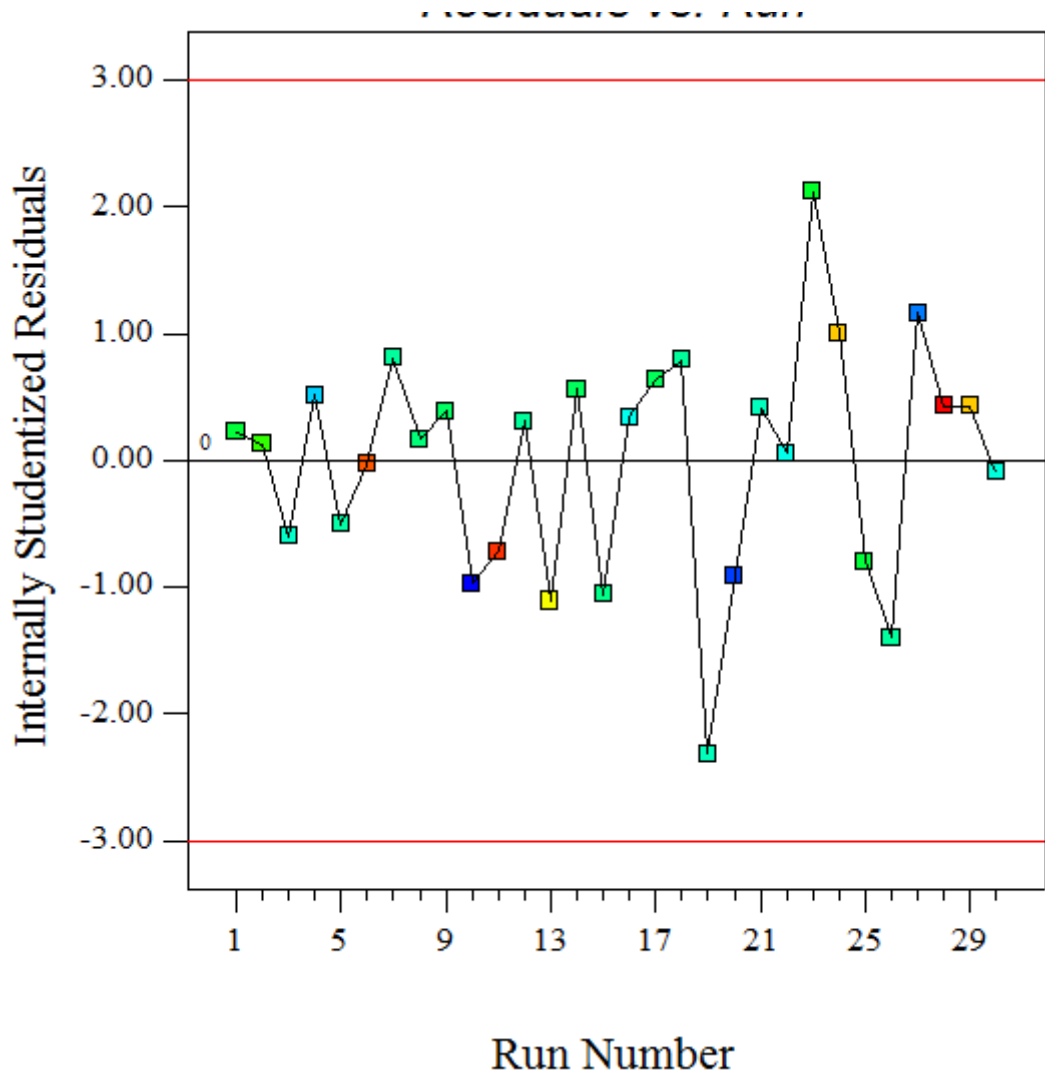
**Figure 6**

The plot of residuals versus run numbers.
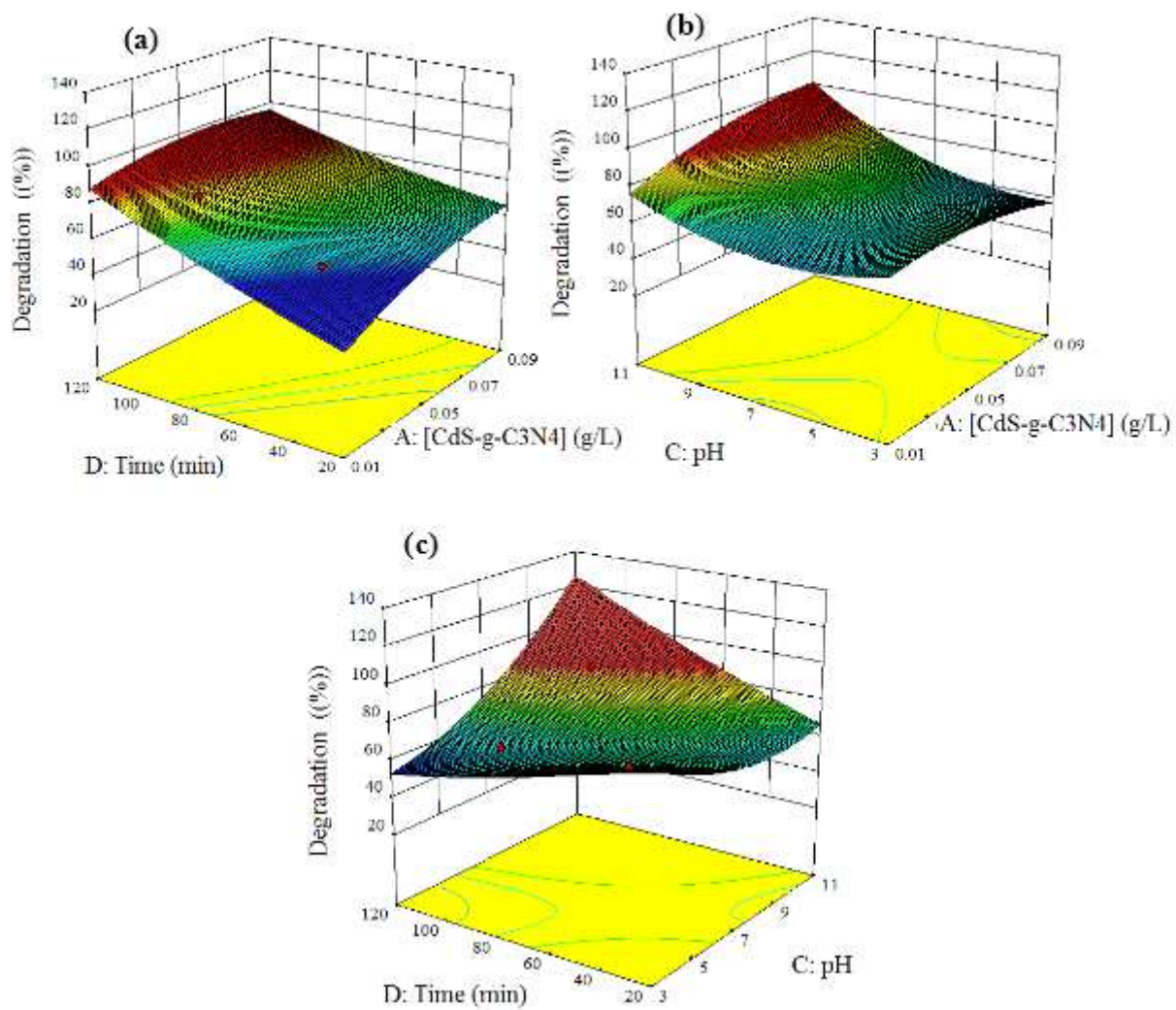
Figure 7

Response surface plots of the CTX photodegradation percentage as a function of (a) concentration of CdS-g-C3N4 nanocomposite and time (b) concentration of CdS-g-C3N4 nanocomposite and pH (c) time and pH.
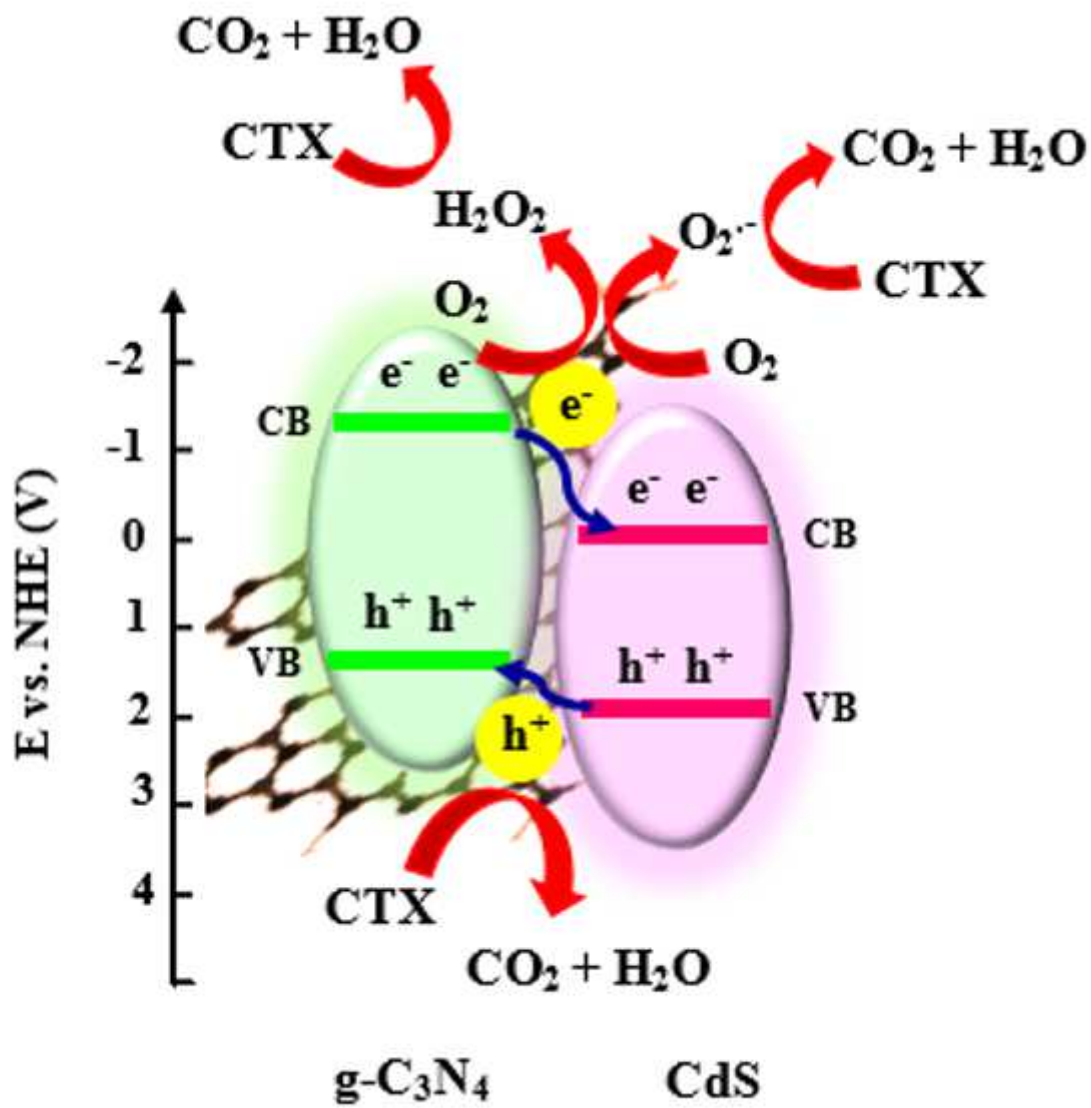
Figure 8

The schematic illustration of photodegradation mechanism for CTX decomposition using CdS-g-C3N4 photocatalyst under visible light.

$$y = 0.0336x + 0.1375$$
$$R^2 = 0.9921$$
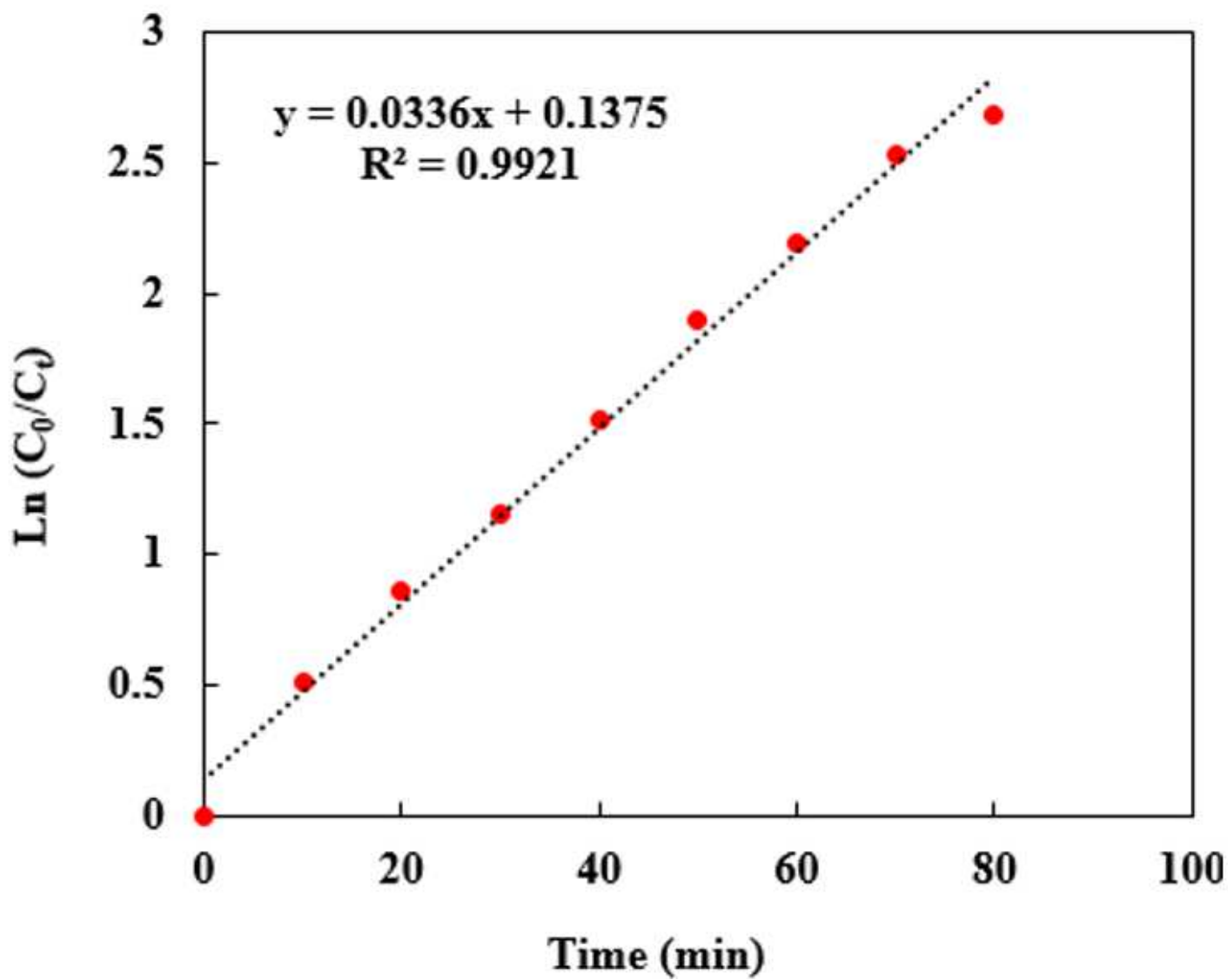
Figure 9

Please see the Manuscript Doc file for the complete figure caption.